,, Caius Iacob" **Conference on**
Fluid Mechanics&Technical Applications
Bucharest, Romania, November 2005

Stability and Bifurcations in the Electroconvection of Nematic Liquid Crystals

by

Iuliana OPREA [1] and Gerhard DANGELMAYR[2]

Abstract

Electroconvection in nematic liquid crystals is a paradigm for pattern formation in anisotropic systems, exhibiting a complex spatiotemporal dynamical structure. We present here the result of a bifurcation study of the motion of a planar layer of nematic liquid crystals subjected to a transverse electric field. The linear stability problem is solved analytically for the velocity and electric potential. Ginzburg Landau type amplitude equations are then used for the weakly nonlinear analysis near threshold. A rich variety of patterns, like travelling waves and rectangles, standing rectangles and rolls, alternating waves and more complex spatiotemporal structures, is predicted at Hopf bifurcation. Eckhaus instability boundaries for these patterns are determined, too.

1 Introduction

Electroconvection(EC) in nematic liquid crystals(NLC) is a pattern forming process related to the anisotropic properties of the liquid crystal. NLC differ from ordinary, isotropic liquids by the fact that the molecules they consist of are on average locally oriented along a preferred direction, called the director. For EC, the NLC is sandwiched between two glass electrode plates and an electric potential difference is applied across the layer. Above a critical value V_c of the applied ac voltage an electrohydrodynamic instability may occur as a transition from the uniform state to a variety of patterns. At onset one typically observes periodic patterns of convection rolls - normal or oblique rolls, depending on the frequency. With increasing voltage transitions take place either to complex spatiotemporal states, induced by defects, or to more complicated quasi-periodic patterns (see [11] for a review).

The traditionally used mathematical model to describe the electrohydrodynamic instability in NLC is the so-called standard model (SM) [10, 17], that combines the continuum theory of Ericksen and Leslie with the quasistatic Maxwell equations in the hypothesis that the charge conduction in the liquid crystal is ohmic. The SM is capable to capture several phenomena observed near threshold of *ac*-driven EC in planarly aligned nematics (e.g. normal, oblique and dielectric rolls, the structure and dynamics of defects), however, it does not exhibit an oscillatory instability which gives rise to the travelling wave patterns frequently observed near onset. Since experiments have shown that the

[1]Faculty of Mathematics, University of Bucharest
E-mail: juliana@math.colostate.edu
[2]Department of Mathematics, Colorado State University

electrical conductivity of NLC is non-ohmic [8], this suggested that the dynamics of ion recombination and dissociation may play a significant role in this system and led to the development of the weak electrolyte model (WEM) [14, 13]. The WEM is an extension of the SM, in which a slow dissociation-recombination of the current-carrying ions is taken into account. This additional process requires to treat the local conductivity σ as a further dynamic variable, an can lead to a distinctive change of the threshold behavior of the electrohydrodynamic instability.
In this work we present results of a nonlinear stability and bifurcation analysis of the weak electrolyte model. The paper is organized as follows. Section 2 describes the basic equations for the rescaled WEM in the limit of zero charge relaxation and constant external electric field. Section 3 presents the linear stability analysis. The linear stability problem is solved analytically for the velocity and electric potential. In Section 4 Ginzburg Landau type amplitude equations are introduced and then used for the weakly nonlinear bifurcation analysis near threshold. A rich variety of patterns, like travelling waves and rectangles, standing rectangles and rolls, alternating waves and more complex spatiotemporal patterns is predicted at Hopf bifurcation. Codimension two bifurcation is found and analyzed, and bounds for the Eckhaus instability are given. We conclude in Section 5 with a short discussion on the results of the computations and open problems.

2 The Weak Electrolyte Model for Electroconvection in Nematic Liquid Crystals

Nematic liquid crystals are charge carrying fluids with long range, uniaxial orientation and molecular alignment, giving rise to anisotropic macroscopic properties. Local orientation of molecules is macroscopically described by the director field $\mathbf{n}$. The external electric field causes the instability of the equilibrium state, leading to electroconvective motion. The standard situation is a layer of nematic liquid crystals sandwiched between two horizontal plates with planar alignment of the director. An applied voltage induces an external alternating electric field in the z–direction. Usually the aspect ratios are large and can be idealized to be infinite, thus the layer is considered to be infinitely extended in the (x, y)–directions. In the approximation of a linear recombination term and of zero diffusivity, the evolution equations of WEM for the local conductivity σ, the internally generated electric potential Φ, the velocity $\mathbf{v}$, pressure p and the director $\mathbf{n}$ ($|\mathbf{n}| = 1$) in dimensionless units are [14, 13]: the ion dissociation–recombination dynamics

$$(\partial_t + \mathbf{v}\cdot\nabla)\sigma \;=\; -\alpha^2\pi^2\nabla\cdot(\mu\mathbf{E}\rho) - \frac{r}{2}(\sigma^2 - 1 - P_1\pi^2\alpha\rho^2), \tag{1}$$

the equation for the director $\mathbf{n}$

$$(\partial_t + \mathbf{v}\cdot\nabla)\mathbf{n} = \omega\times\mathbf{n} + \mathbf{d}(\lambda\mathbf{A}\mathbf{n} - \mathbf{h}), \tag{2}$$

the conservation of charge

$$P_1(\partial_t + \mathbf{v}\cdot\nabla)\rho \;=\; -\nabla\cdot(\mu\mathbf{E}\boldsymbol{\sigma}), \tag{3}$$

together with the Poisson's law for the electric charge density ρ,

$$\rho = \nabla\cdot(\epsilon\mathbf{E}), \tag{4}$$

and the generalized Navier Stokes equations

$$P_2(\partial_t + \mathbf{v}\cdot\nabla)\mathbf{v} = -\nabla p - \nabla\cdot(\mathbf{T}+\mathbf{\Pi}) + \pi^2\rho\mathbf{E}, \quad (5)$$

$$\nabla\cdot\mathbf{v} = 0, \quad (6)$$

where $\mathbf{E} = (\sqrt{2R}/\pi)\cos(\omega_0 t)\mathbf{e}_3 - \nabla\Phi$ is the electric field, $\omega = 1/2(\nabla\times\mathbf{v})$ is the vorticity, and $\mathbf{A}$, with components $A_{ij} = \frac{1}{2}(v_{i,j} + v_{j,i})$, is the strain tensor. We use the scaling introduced in [14] in which lengths, time, orientational elasticities, viscosities, dielectric permittivities, and voltages are measured in units of d/π (d: distance between the plates), director relaxation time τ_d, splay deformation constant K_1, $\gamma_1 = \tilde{\alpha}_3 - \tilde{\alpha}_2$, $\epsilon_0\epsilon_\perp$, and V_c, respectively, where

$$\tau_d = \frac{\gamma_1 d^2}{K_1\pi^2}, \quad V_c = \sqrt{\frac{K_1\pi^2}{\epsilon_0\epsilon_\perp}},$$

and $\epsilon_0\epsilon_\perp(\delta_{ij} + \varepsilon_a n_i n_j)$ and $\tilde{\alpha}_j$ $(1 \le j \le 6)$ are the unscaled dielectric permittivity tensor and the Leslie coefficients, respectively. The Prandtl-type number P_2 is the ratio $P_2 = \tau_{visc}/\tau_d$, where $\tau_{visc} = d^2\rho_m/\gamma_1$ is the viscous relaxation time and ρ_m is the mass density. The Prandtl-type number P_1 is the ratio of the charge relaxation time and the director relaxation time, $P_1 = \tau_q/\tau_d$, where $\tau_q = \epsilon_0\epsilon_\perp/\sigma_\perp$ and $\sigma_{i,j} = \sigma_\perp + \sigma_a n_i n_j$ is the conductivity tensor $\boldsymbol{\sigma}$. Conductivities are measured in units of the equilibrium conductivity $\sigma_{eq} = (\mu^+ + \mu^-)en_0$, defined in terms of the mobilities $\mu^\pm$, the elementary charge e and the equilibrium concentration n_0 of the ions. The parameters α, r are given by [14]

$$\alpha = \sqrt{\frac{\mu^+\mu^-\gamma_1\pi^2}{\sigma_{eq}d^2}}, \quad r = \frac{\tau_d}{\tau_{rec}},$$

with the recombination time $\tau_{rec} = (2k_r n_0)^{-1}$, k_r being the recombination constant. Both of these parameters are also Prandtl–type time scale ratios.

The units are normalized such that the height of the layer is π. Using the common planar alignment, the coordinate system is chosen such that $\mathbf{n} = (1,0,0)$ at the upper and lower plates located at $z = \pm\pi/2$. The 'rigid' boundary conditions on top and bottom of the layer,

$$\frac{\partial\sigma}{\partial z}, n_2,\ n_3,\ \phi,\ \mathbf{v} = 0 \text{ at } z = \pm\pi/2, \quad (7)$$

are deduced from the ideal conducting plates condition, rigid anchoring for the director, and finite viscosity. The molecular field

$$\mathbf{h} = (\frac{\partial f}{\partial\mathbf{n}} - \nabla\cdot\frac{\partial f}{\partial\nabla\mathbf{n}}) - \varepsilon_a\pi^2(\mathbf{n}\cdot\mathbf{E})\mathbf{E},$$

is derived from the elastic energy density,

$$2f = K_1(\nabla\cdot\mathbf{n})^2 + K_2[\mathbf{n}\cdot(\nabla\times\mathbf{n})]^2 + K_3[\mathbf{n}\times(\nabla\times\mathbf{n})]^2,$$

due to splay (K_1), twist (K_2), and bend (K_3) deformations – in our scaling the splay deformation coefficient K_1 is normalized to unity. The tensors μ, ϵ, $\mathbf{d}$, $\mathbf{T}$, Π are the scaled mobility, dielectric, projection, viscous stress and Erickson stress tensor, with components

$$\mu_{ij} = \delta_{ij} + \sigma_a n_i n_j, \quad \epsilon_{ij} = \delta_{ij} + \epsilon_a n_i n_j, \quad d_{ij} = \delta_{ij} - n_i n_j,$$

$$-T_{ij} = \alpha_1 n_i n_j n_k n_l A_{kl} + \alpha_2 n_j N_i + \alpha_3 n_i N_j + \alpha_4 A_{ij} + \alpha_5 n_j n_k A_{ki} + \alpha_6 n_i n_k A_{kj}, \;\; \Pi_{ij} = \frac{\partial f}{\partial n_{k,j}} n_{k,i}$$

where $\mathbf{N} = \mathbf{d}(\lambda \mathbf{A}\mathbf{n} - \mathbf{h})$. The scaled Leslie coefficients $\alpha_1, \ldots, \alpha_6$ ($\alpha_j = \tilde{\alpha}_j/\gamma_1$) and the Onsager coefficient λ in (2) satisfy the Onsager relations $\alpha_1 + \alpha_3 = \alpha_6 - \alpha_5$, $\alpha_3 - \alpha_2 = 1$, and $\lambda = \alpha_5 + \alpha_6$. We introduce the independent parameters (Miesowicz coefficients)

$$\eta_0 = \alpha_1 + \alpha_4 + \alpha_5 + \alpha_6, \; \eta_1 = (-\alpha_2 + \alpha_4 + \alpha_5)/2, \; \eta_2 = (\alpha_3 + \alpha_4 + \alpha_6)/2, \; \eta_3 = \alpha_4/2,$$

and use the Onsager relations to express $\lambda, \alpha_1, \ldots, \alpha_6$ in terms of the four independent Miesowicz coefficients $\eta_0, \eta_1, \eta_2, \eta_3$. as

$$\lambda = \eta_1 - \eta_2, \; \alpha_1 = \eta_0 - 2\eta_1 - 2\eta_2 + 2\eta_3 + 1, \; \alpha_2 = -(1+\lambda)/2, \; \alpha_3 = (1-\lambda)/2,$$

$$\alpha_4 = 2\eta_3, \; \alpha_5 = 2\eta_1 - 2\eta_3 - (1+\lambda)/2, \; \alpha_6 = 2\eta_2 - 2\eta_3 - (1-\lambda)/2.$$

The system (1)–(7) depends on the main bifurcation parameters R and ω_0 (amplitude and frequency of the external field), four Prandtl–type time scale ratios P_1, P_2, (viscous and charge relaxation time to director relaxation time), α (mobility parameter) and r (recombination parameter), dielectric and conductivity anisotropy coefficients ε_a and σ_a, and the material parameters $K_2, K_3, \eta_0, \eta_1, \eta_2, \eta_3$. The system (1)–(7) has reflectional

$$\begin{aligned} (x, n_2, n_3, v_1) &\rightarrow (-x, -n_2, -n_3, -v_1) \\ (y, n_2, v_2) &\rightarrow (-y, -n_2, -v_2) \\ (z, n_3, v_3, \Phi) &\rightarrow (-z, -n_3, -v_3, -\Phi) \end{aligned}$$

and translational

$$(x, y) \rightarrow (x + \xi, y + \eta)$$

symmetries (fields that preserve their signs are suppressed) due to the assumption of an infinitely extended layer in x and y, but there are no rotational symmetries due to the anisotropy of the system. The resulting symmetry group is $E_1 \times E_1 \times Z_2$ and the compactified symmetry group, in case of periodic boundary conditions in (x, y), is $O(2) \times O(2) \times Z_2$.

The equations (1)–(7) are extremely complicated, and full 3-d simulations for large aspect ratios are still beyond the scope of present day's supercomputers. Thus a weakly nonlinear analysis near onset is particularly useful, and is appreciated by experimentalists.

Typically the Prandtl numbers P_1, P_2 are very small compared to the other parameters, at least in the conduction range, thus one can take the limit $P_2 = 0$ (zero viscous relaxation time) and $P_1 = 0$ (zero charge relaxation time). Partial results of a weakly nonlinear analysis of the WEM in this approximation, in which the z-dependence of the velocity was approximated by two Chandrasekhar modes and only three Fourier modes have been taken into account, have been presented in [13] for the case of a Hopf bifurcation with only two minima of the neutral stability surface (see Section 4.2). The theoretical results were in good agreement with some experiments [8, 9], but still more accurate numerical computations as well as computations for other parameters and other types of instabilities are necessary to test the validity of the WEM.

3 Linear stability analysis

We consider the WEM equations (1)–(7) in the limit of zero viscous and charge relaxation time $P_1 = P_2 = 0$ and we assume a constant external electric field in the z-direction ($\omega_0 = 0$). In this limit the equations (1)–(6) split into the evolution equations for the variables σ and $\mathbf{n}$

$$(\partial_t + \mathbf{v}\cdot\nabla)\sigma = -\alpha^2\pi^2\nabla\cdot(\mu\mathbf{E}\rho) - \frac{r}{2}(\sigma^2-1), \tag{8}$$

$$(\partial_t + \mathbf{v}\cdot\nabla)\mathbf{n} = \omega\times\mathbf{n} + \mathbf{d}(\lambda\mathbf{A}\mathbf{n} - \mathbf{h}), \tag{9}$$

and the equations for $\mathbf{v}$, p and Φ

$$-\nabla p - \nabla\cdot(\mathbf{T}+\mathbf{\Pi}) + \pi^2\rho\mathbf{E} = 0, \qquad \nabla\cdot\mathbf{v} = 0, \tag{10}$$

$$-\nabla\cdot(\mu\mathbf{E}\sigma) = 0, \tag{11}$$

with

$$\rho = \nabla\cdot(\epsilon\mathbf{E}), \qquad \mathbf{E} = (\sqrt{2R}/\pi)\mathbf{e}_3 - \nabla\Phi. \tag{12}$$

The remaining parameters are the material and WEM parameters $K_2, K_3, \eta_0, \eta_1, \eta_2, \eta_3$, α, r, ε_a, σ_a, and the bifurcation parameter R measuring the external electric field strength. Substituting (12) into (8)–(11) leads to a system of equations for the 'dynamical variables' σ, n_2, n_3 ($|\mathbf{n}| = 1$) and for the 'slave variables' Φ and $\mathbf{v} = (v_1, v_2, v_3)$.
The basic state of (1)–(7) is given by $\sigma = 1$, $\mathbf{v} = 0$, $\Phi = 0$, $\mathbf{n} = (1, 0, 0)$, p = *const*. The stability of this state is governed by linearized equations for perturbational fields $\delta\sigma$, δn_2, δn_3, $\delta\phi$, $\delta v_j, j = 1,\dots 3$, δp. Owing to the translation invariance w.r.t. (x, y), the perturbational fields are represented by horizontal Fourier modes,

$$(\delta\sigma, \delta n_2, \delta n_3, \delta\phi, \delta v_j, \delta\mathrm{p}) = e^{i(px+qy)}(\Sigma, N_2, N_3, \Phi, V_j, \mathrm{P}),$$

where Σ, N_2 etc. depend on (t, z, p, q) and the parameters. The velocities V_j are represented by poloidal and toroidal stream functions F and G leaving us with a system of linear equations for $(\Sigma, N_2, N_3, \Phi, F, G)$. With the notations $D = (\Sigma, N_2, N_3)$, $S = (\Phi, F, G)$ the linearized WEM equations can be written symbolically as

$$D_t = \mathcal{L}_D(D,S) \equiv \mathcal{L}_{DD}(p,q,R)D + \mathcal{L}_{DS}(p,q,R)S \tag{13}$$

$$0 = \mathcal{L}_S(D,S) \equiv \mathcal{L}_{SD}(p,q,R)D + \mathcal{L}_{SS}(p,q,R)S \tag{14}$$

where $\mathcal{L}_D = (\mathcal{L}_\Sigma, \mathcal{L}_{N_2}, \mathcal{L}_{N_3})$, $\mathcal{L}_S = (\mathcal{L}_\Phi, \mathcal{L}_F, \mathcal{L}_G)$ are linear differential operators w.r.t. z. The expressions of $\mathcal{L}_D, \mathcal{L}_S$ and the other operators in (13), (14) are given in the Appendix. The boundary conditions (7) in the new variables read as

$$\Sigma_{,3} = N_2 = N_3 = 0, \quad F = F_{,3} = G = 0 \qquad \text{at} \qquad z = \pm\pi/2. \tag{15}$$

Formally, (13)-(14) form a linear dynamical system for D,

$$D_t = L(D|p,q,R), \tag{16}$$

obtained by solving (14) for $S(D|p,q,R) = -\mathcal{L}_{SS}^{-1}\mathcal{L}_{SD}D$ and substituting this into (13). Since the solution $S(D|p,q,R)$ with the given boundary conditions is represented by an integral operator, $L = (\mathcal{L}_{DD} - \mathcal{L}_{DS}\mathcal{L}_{SS}^{-1}\mathcal{L}_{SD})$ is an integro–differential operator with respect to z. The solution of (14) is facilitated by the fact that the Φ–component does not depend on the velocity.
Neutral stability of the basic state occurs on a neutral stability surface in (p,q,R)–space on which L has either a zero eigenvalue (stationary neutral stability surface SNSS) giving rise to a stationary bifurcation, or a purely imaginary eigenvalue (oscillatory neutral stability surface ONSS) giving rise to a Hopf bifurcation. The transition to instability occurs at minimum (p_c, q_c, R_c) of lower neutral stability surface.
To obtain a Galerkin approximation of L w.r.t. D we use natural, adapted to the boundary conditions, sine- and cosine vertical modes. Due to the z-reflectional symmetry L has odd and even invariant subspaces spanned by modes of the form $D_m = (a_1 \sin(2m-1)z, a_2 \sin 2mz,\ a_3 \cos(2m-1)z)$, $m \geq 1$ odd, and $E_m = (a_1 \cos 2mz,\ a_2 \cos(2m+1)z, a_3 \sin 2mz)$, $m \geq 0$ even, respectively. For the parameter range considered here the instability occurs in the odd subspace. In this subspace L is represented by an infinite matrix $\mathcal{M}$ composed of 3×3 blocks $M(m,n)$ defined by

$$M_{ij}(m,n) = (2/\pi)\int_{-\pi/2}^{\pi/2} L(D_{mi}) \cdot D_{nj} dz, \quad 1 \leq i,j, \leq 3, \tag{17}$$

where D_{mi} is the D_m mode with $a_j = \delta_{ij}$. To find these matrices, for any mode D_m we obtain the exact solution $S_m = S(D_m|p,q,R)$ of the nonhomogeneous equations (14) subjected to corresponding boundary conditions and then evaluate the resulting integral (17) analytically. The solution of the Φ–equation is straightforward and preserves the chosen modes. In contrast, the solution of the F and G–equations involves hyperbolic functions leading to a transcendental dependence of the M_{ij} on (p,q). We note that, due to the anisotropy and the rigid boundary conditions, these analytical computations are not trivial.
To compute the critical data (p_c, q_c, R_c) numerically we used a $3N \times 3N$ truncation of $\mathcal{M}$ by restricting (m,n) to $1 \leq m,n \leq N$. We move progressively to higher values of N, using the previously computed values as starting values for the numerical search. The task of determining the local form of the critical eigenvalue near the minimum of the ONSS involves a three parameter Hopf computation. For $N = 1$, the analytically derived equations for an imaginary eigenvalue of a 3×3 matrix and for a minimum of R are solved numerically and the results are used as a starting value for the calculations with $N > 1$, for which the ONSS is computed with the Werner's augmented system [16] and minimized using a Nelder–Mead method [1]. We have first reproduced the calculations done by [14] for the $q_c = 0$-case. Numerical convergence with an accuracy up to five significant figures was usually observed for $N \geq 9$. We computed the neutral stability surface for values of parameters corresponding to two nematics MBBA and I52 [4] and we found steady as well as Hopf bifurcation with $q_c \neq 0$, which complements the results of [14] and explain the oblique rolls observed experimentally.

4 Weakly nonlinear analysis

4.1 Ginzburg Landau Formalism for two-dimensional anisotropic systems.

Instabilities of homogeneous states in spatially extended systems are usually described by envelope or modulation equations of the Ginzburg Landau type. Like normal forms for ODEs and maps, the form of these equations is mainly determined by the symmetries of the governing PDEs and the type of instability (see [2, 7, 6]). We refer to this approach to studying instabilities in extended systems in terms of canonical envelope equations as 'Ginzburg Landau formalism'.
The weak electrolyte model is a particular case of an axially anisotropic, dissipative systems with two extended dimensions (x, y). In such systems, the axial anisotropy induces reflection and translation invariancy in both extended directions, thus the underlying symmetry group is $E(1) \times E(1)$ which compactifies to $O(2) \times O(2)$ if periodic boundary conditions are imposed. The standard situation is that a homogeneous basic solution of a system of PDE's for physical variables $\mathbf{u} = (u_1, u_2, \ldots)$ becomes unstable if a bifurcation parameter R exceeds a threshold R_c. Typically, $R_c = R(p_c, q_c)$ is the minimum of a neutral stability surface (NSS) $R(p, q)$, on which the basic state is marginally stable against plane wave perturbations with wave numbers (p, q). The NSS is derived from $\mu_r(p, q, R) = 0$, where $\mu(p, q, R) = \mu_r(p, q, R) + i\omega(p, q, R)$ is the critical eigenvalue of the linearized system. The threshold values (p_c, q_c) and $\omega_c = \omega(p_c, q_c, R_c)$ are referred to as the critical wave numbers and frequency, respectively. By means of a multiple scale expansion one can derive a system of evolution equations (Ginzburg Landau equations) for slowly varying envelopes that modulate the dynamics of bifurcated solutions of the linearized problem near onset.
In the next section we will introduce the systems of Ginzburg Landau equations for two-dimensional anisotropic systems in the case of four minima of the neutral stability surface, used in the weakly nonlinear analysis of the WEM.

4.2 Globally Coupled Ginzburg Landau Equations

In the following we focus on the Hopf bifurcation in anisotropic systems with four minima of the neutral stability surface, and hence four critical wave numbers $(\pm p_c, \pm q_c)$. These wave numbers define two oblique ('zig' and 'zag') directions for two pairs of counterpropagating travelling waves of the linearized equations at onset. The solution of the underlying PDE system near onset, here (8)–(11), is represented by a superposition of the two pairs of waves in the form

$$\begin{aligned}\mathbf{u}(t, x, y, z) &= (\mathcal{A}_1 e^{i(p_c x + q_c y)}\mathbf{U}_1(t, z) + \mathcal{A}_2 e^{i(-p_c x + q_c y)}\mathbf{U}_2(t, z) + \mathcal{A}_3 e^{i(-p_c x - q_c y)}\mathbf{U}_3(t, z) \\ &\quad + \mathcal{A}_4 e^{i(p_c x - q_c y)}\mathbf{U}_4(t, z))e^{i\omega_c t} + \text{cc} + \text{h.o.t.}, \end{aligned} \tag{18}$$

(cc = complex conjugate) where the $\mathcal{A}_j, j = 1 \ldots n$ are small, slowly varying envelopes, and h.o.t. refers to terms of higher order in $R - R_c$ and the $\mathcal{A}_j$ and their derivatives. The $\mathbf{U}_j(t, z)$ are the (symmetry related) critical modes which are T_e–periodic in case of periodic systems, and, if present in the original PDE, may depend on a further, bounded space variable z.
By means of a formal expansion in the $\mathcal{A}_j$ and their derivatives, as well as symmetry considerations,

one can derive a system of modulation equations or the envelopes[3]. The equation for $\mathcal{A}_1$ reads,

$$\mathcal{A}_{1t} + v_x\mathcal{A}_{1x} + v_y\mathcal{A}_{1y} = [a_0(R-R_c) + \widetilde{\mathcal{D}}(\partial_x, \partial_y) + \sum_{j=1}^{4} a_j|\mathcal{A}_j|^2]\mathcal{A}_1 + a_5\mathcal{A}_2\bar{\mathcal{A}}_3\mathcal{A}_4 + \text{h.o.t.}, \qquad (19)$$

where $(v_x, v_y) = \nabla\omega|_c$ are the critical group velocities, $a_0, a_1, \ldots, a_5$ are complex coefficients, and $\widetilde{\mathcal{D}}$ is a complex second order differential operator in (∂_x, ∂_y) with elliptic real part. The linear coefficients $(v_x, v_y, a_0,$ and coefficients of $\widetilde{\mathcal{D}})$ in (19) are determined by the first and second order expansion coefficients of the critical eigenvalue μ about criticality, and the nonlinear coefficients a_j, $1 \le j \le 5$, are determined by the quadratic and cubic terms of the given PDE system. The h.o.t. in (19) refers to higher order terms which do not contribute at leading order when (19) is rescaled and expanded in powers of $\varepsilon = \sqrt{R-R_c}$. The equations for $\mathcal{A}_2, \mathcal{A}_3, \mathcal{A}_4$ follow from (19) through appropriate reflection operations.

The system (19) is still in unscaled form. The usual scaling $R - R_c = \varepsilon^2$, $T = \varepsilon^2 t$, $\mathcal{A}_j(t,x,y) = \varepsilon A_j(T, \varepsilon x, \varepsilon y)$, would lead to a system of four locally coupled Ginzburg Landau equations, provided the group velocities are small (order $O(\varepsilon)$). In the generic case in which v_x, v_y are of order 1, one has to resort to four slow wave variables $\xi_\pm = \varepsilon(x \pm v_x t)$, $\eta_\pm = \varepsilon(y \pm v_y t)$, adapted to the first order wave operator on the left hand side of (19). It can be shown [3] that a consistent expansion $\mathcal{A}_j = \varepsilon A_j + O(\varepsilon^2)$ requires that A_1, A_2, A_3, A_4 depend on T and (ξ_+, η_+), (ξ_-, η_+), (ξ_-, η_-), (ξ_+, η_-), respectively, and that the A_j satisfy a system of four globally coupled Ginzburg Landau equations. The equation for A_1 is given by

$$\begin{aligned} A_{1T} \;=\; & \{a_0 + \mathcal{D}(\partial_{\xi_+}, \partial_{\eta_+}) + a_1|A_1|^2 + a_2 < |A_2(s,\eta_+)|^2 > \\ & + a_3 < |A_3(\xi_+ + s, \eta_+ + s)|^2 > + a_4 < |A_4(\xi_+, s)|^2 > \} A_1 \\ & + a_5 < A_2(\xi_+ + s, \eta_+)\bar{A}_3(\xi_+ + s, \eta_+ + s)A_4(\xi_+, \eta_+ + s) >, \end{aligned} \qquad (20)$$

where $\mathcal{D}$ is a rescaled version of $\widetilde{\mathcal{D}}$, and the brackets denote averages over s. The equations for A_2, A_3, A_4 follow again from (20) through appropriate reflection operations. The meaning of the global coupling terms is that fast energy transport due to finite group velocities causes wave interactions to occur on average rather than locally in space.

4.3 Solutions of the Globally Coupled Ginzburg Landau Equations

If spatial variations are ignored, the globally coupled system for the A_j reduces to the normal form for a Hopf bifurcation with $O(2) \times O(2)$ symmetry,

$$\frac{dA_1}{dT} = (a_0 + \sum_{j=1}^{4} a_j|A_j|^2)A_1 + a_5 A_2\bar{A}_3 A_4. \qquad (21)$$

with the equations for A_2, A_3, A_4 following by applying the permutations $(2,1,4,3)$, $(3,1,4,2)$, $(4,3,2,1)$ to the indices of the A_j in (21) [12, 15]. The normal form (21) has six basic solutions corresponding to six basic wave patterns shown by $\mathbf{u}(t,x,y,z)$ when represented by (18): travelling and standing waves (TW and SW), two types of travelling rectangles (TR), standing rectangles

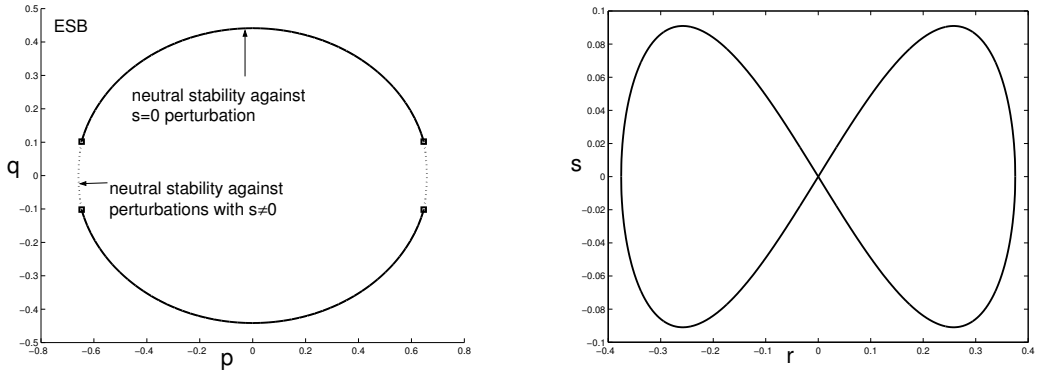

(a) (b)

Figure 1: An Eckhaus stability boundary for TW.

(SR), and alternating waves (AW), which alternate periodically between differently oriented standing waves. The dynamical repertoire of (21) is rich and not yet fully explored, but several facts are known. First, several (up to three) basic wave patterns can be simultaneously stable. Second, there are eight four–dimensional invariant subspaces and in one of them we can find quasiperiodic solutions. Third, several heteroclinic cycles connecting different basic periodic solutions can occur as attractors in certain parameter regimes.

The basic periodic solutions of (21) that reside in two–dimensional fixed point subspaces induce wave solutions of the original system with critical wave numbers (p_c, q_c). The globally coupled system of complex Ginzburg Landau equations (20) allows to extend these solutions to families of wave solutions with nearby critical wave numbers $(p_c + \varepsilon p, q_c + \varepsilon q)$. If a basic wave pattern appears stably as solution of (21), the Eckhaus stability boundary (ESB) for fixed $R > R_c$ is a closed curve in the (p, q) plane that separates stable (interior of ESB) and unstable solutions of the family.

In [5] we have analysed the ESB's for travelling waves. The analysis for all the six wave patterns is algebraically very complicated due to the fact that the ESB of a particular wave pattern depends on all six coefficients of the differential operator $\mathcal{D}$ as well as on certain combinations of the a_j. Our preliminary results show that in certain parameter regimes finite wavelength instabilities are dominant. For example, in Figure 1(a) we display a possible form of the TW–ESB. In this figure, wave vectors (p, q) in the interior of the ESB–curve give rise to Eckhaus stable TW's. On the solid part of the ESB–curve we find long wavelength instabilities, and on the dotted part the TW is neutrally stable against wave vectors (r, s) located on the figure 8 curve shown in Figure 1(b). For other parameters either the solid or the dotted part disappears.

4.4 Numerical computation of the coefficients $a_1, \ldots, a_5$ for the weak electrolyte model and numerical results

We analyze the wave patterns shown by (20) and their stability in the case of the weak electrolyte model in order to predict stable electroconvective wave patterns near onset. The computation of the

nonlinear coefficients a_j in the globally coupled Ginzburg Landau equations (20) or (21) proceeds by numerically evaluating their analytical representation in terms of the bilinear and cubic terms of the WEM equations (13)-(14) with an adjoint critical mode. This involves solving a hierarchy of nonhomogeneous linear equations, where at each stage the (14)–equations are inverted numerically using the Green's matrix.

The WEM equations depend on the bifurcation parameter R and the ten (dimension less) material and WEM parameters $(K_2, K_3, \varepsilon_a, \sigma_a, \eta_0, \eta_1, \eta_2, \eta_3, r, \alpha)$. We are looking for parameter regimes where the first instability when R increases is a Hopf bifurcation at $R = R_c$, with nonzero critical wave numbers (p_c, q_c), the case of interest for experimentalists. In our numerical investigation we varied K_2, K_3 (ratios of the twist and bend distortion coefficients to the splay distortion coefficient), and kept the remaining eight material parameters fixed. The SM–parameters $(\varepsilon_a, \sigma_a, \eta_0, \eta_1, \eta_2, \eta_3)$ have been matched to measured values of the materials I52 and MBBA at room temperature, as in [14]. The values of the WEM–specific parameters r and α have been chosen such that a Hopf bifurcation with $q_c \neq 0$ occurs. Figure 2 summarizes the results of the weakly nonlinear analysis in the form of a

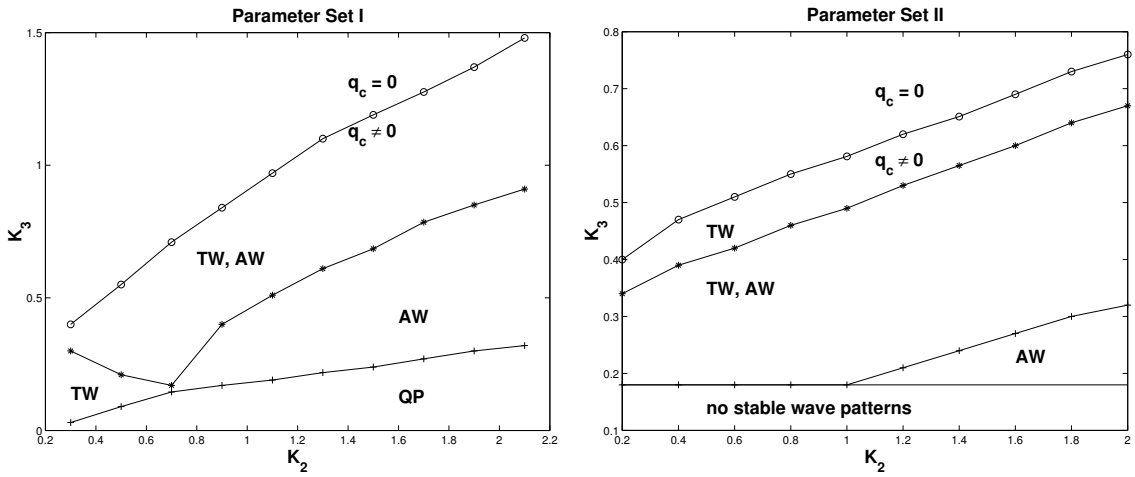

Figure 2: Stable wave patterns for the WEM predicted by (21).

stability diagram in the (K_1, K_2)–plane (I:I52, II:MBBA). For a given value of K_2, we first computed a value $K_3 = K_{3d}(K_2)$ such that for K_3 above K_3 the transverse critical wave number q_c is zero, and below it is nonzero. The points $K_3 = K_{3d}(K_2)$ define the locus of a codimension two bifurcation for which the two NSS minima on the p–axis degenerate in the q–direction. For $K_3 < K_{3d}(K_2)$ we find different basic wave patterns occurring stably as solutions of (21) in different regions as marked in the diagrams. Note that for both parameter sets there is a certain range where TW and AW are simultaneously stable. Moreover, the parameter scans indicate the presence of a codimension three point that organizes transitions between TW and AW as well as the disappearance of stable basic patterns for small values of K_3. While in this range for set I the basic periodic solutions TW and AW are replaced by temporally quasiperiodic solutions (QP) residing in four dimensional invariant subspaces, the dynamics for small K_3 in case of set II has not yet been identified. We assume that

here the attractors of (21) are heteroclinic cycles or higher dimensional tori.

5 Conclusions

In this paper we have analyzed stable wave patterns predicted by a Hopf bifurcation with four critical wave numbers $(\pm p_c, \pm q_c)$, each corresponding to an oblique travelling roll solution of the linearized WEM equations at onset. The method we developed provides a systematic analysis of the bifurcated solutions and their stability. In this investigation we varied (K_2, K_3) and kept the other material parameters fixed. Our numerical findings suggest that travelling rolls and alternating waves play a dominant role. We have considered the case of a constant electric field. If the external field is time-periodic (ac-field), the governing equations represent a parametrically forced nonautonomous system, and averaging methods must be used prior to a bifurcation analysis. Results of a similar analysis with nonzero driving frequency ω_0 of the external field will presented in a future work.

6 Appendix

The linearized WEM equations depend on several anisotropic horizontal differential operators which become polynomials in (p, q) after Fourier transformation. To obtain a compact representation of these polynomials we introduce basic polynomials of the form $k_j^2 = c_p p^2 + c_q q^2$ $(0 \le j \le 12)$ in Table 1. The parameters a, b, c, η occurring in this table are defined by

$$a = \eta_0, \;\; b = \frac{1}{4}[2(\eta_1 + \eta_2) - (\eta_1 - \eta_2)^2 - 1], \;\; c = \eta_3, \;\; \eta = \eta_2 - \eta_1.$$

With this notation the linearized equations for Σ, N_2, N_3 take the form (prime denotes ∂_z)

$$\begin{aligned}
\partial_t \Sigma &= -r\Sigma - 2ip\alpha^2 \varepsilon_a R N_3' + \alpha^2 \pi \sqrt{2R}(\partial_z^2 - k_6^2)\Phi', && \text{(A.1)}\\
\partial_t N_2 &= 2(K_3 \partial_z^2 - k_2^2)N_2 - 2iq(K_3 - 1)N_3' - (i/2)L_2(\mathbf{V}), && \text{(A.2)}\\
\partial_t N_3 &= 2(1 - K_3)iqN_2' + 2(\partial_z^2 + \varepsilon_a R - k_3^2)N_3 && \text{(A.3)}\\
&\quad -\varepsilon_a \pi \sqrt{2R} ip\Phi - (1/2)L_3(\mathbf{V}),
\end{aligned}$$

where

$$L_2(\mathbf{V}) = (1+\eta)qV_1 - (1-\eta)pV_2, \;\; L_3(\mathbf{V}) = (1+\eta)V_1' - (1-\eta)ipV_3,$$

and the V_j are expressed through F, G as

$$V_1 = iqG + cipF', \;\; V_2 = -ipG + biqF', \;\; V_3 = k_0^2 F. \qquad \text{(A.4)}$$

Note that (A.4) differs slightly from the commonly used representation of velocities in terms of stream functions. The chosen form turns out to be particularly useful when solving the nonhomogeneous velocity equations.
The linearized equation for the potential reads

$$(\partial_z^2 - k_7^2)\Phi - (\sqrt{2R}/\pi)(\sigma_a ipN_3 + \Sigma') = 0, \qquad \text{(A.5)}$$

and the equations for the stream functions are given by

$$(k_0^4k_1^2 - B\partial_z^2 + bck_0^2\partial_z^4)F - sp^3qG' + \pi\sqrt{2R}(k_9^2\partial_z^2 - k_8^2k_0^2)\Phi + L_F(N_2, N_3) = 0, \tag{A.6}$$

$$(A - k_0^2\partial_z^2)G + sp^3qF' + \varepsilon_a\pi\sqrt{R/2}(1+\eta)pq\Phi' + L_G(N_2, N_3) = 0, \tag{A.7}$$

where $s = ac - 2bc - b^2 + c^2$, $A = bp^4 + (a - 2b + 2c)p^2q^2 + bq^4$, $B = c^2(a - 2b + 2c)p^4 + b(b^2 + 3c^2)p^2q^2 + 2cb^2q^4$, and

$$\begin{aligned} L_F(N_2, N_3) &= pq\{[(1+\eta)c - (1-\eta)K_3b]\partial_z^2 - k_{10}^2\}N_2' \\ &\quad -ip\{c(1+\eta)\partial_z^4 - [k_{12}^2 - (1+\eta)c\varepsilon_aR]\partial_z^2 \\ &\quad +[(1-\eta)k_3^2 + (1+\eta)\varepsilon_aR]k_0^2\}N_3, \\ L_G(N_2, N_3) &= (k_2^2k_4^2 - k_5^2\partial_z^2)N_2 + iq[(1+\eta)(\partial_z^2 + \varepsilon_aR) - k_{11}^2]N_3'. \end{aligned}$$

	k_0^2	k_1^2	k_2^2	k_3^2	k_4^2	k_5^2	k_6^2	k_7^2	k_8^2
c_p	c	b	K_2	K_2	$1-\eta$	$(1-\eta)K_3$	$1+\varepsilon_a$	$1+\sigma_a$	$1+(1+\eta)\frac{\varepsilon_a}{2}$
c_q	b	c	1	K_3	$1+\eta$	$1+\eta$	1	1	1

	k_9^2	k_{10}^2	k_{11}^2	k_{12}^2
c_p	$c-(1+\eta)\frac{c\varepsilon_a}{2}$	$(1+\eta)cK_2 + (1-\eta)(c - bK_2 - cK_3)$	$(1+\eta)K_2 + (1-\eta)(1-K_3)$	$(1+\eta)cK_2 + (1-\eta)c$
c_q	b	$(1+\eta)c-(1-\eta)bK_3$	$1+\eta$	$(1+\eta)c+(1-\eta)bK_3$

Table 1: Coefficients c_p, c_q in $k_j^2 = c_pp^2 + c_qq^2$.

References

[1] E. Allgower and K. Georg and I. Oprea and G. Dangelmayr, Matrix-Free Numerical Computation of Instabilities of Periodic Patterns, in *Dynamics and Bifurcation of Patterns in Dissipative Systems*, World Scientific Series on Nonlinear Sciences, Series B, 20-38,2004

[2] M. Cross and P. Hohenberg, Pattern Formation outside Equilibrium, *Rev. Mod. Phys.*, **65**, 851-1123, 1993

[3] G. Dangelmayr and M. Wegelin,Hopf bifurcations in anisotropic systems,in *Pattern Formation in Continuous and Coupled Systems*, (M. Golubitsky and D. Luss and S. Strogatz eds.), Springer, IMA Vol. in Math. and Appl.**115**, 33-48, 1999

[4] G. Dangelmayr and I. Oprea, A Bifurcation Study of Wave Patterns for Electroconvection in Nematic Liquid Crystals, *Mollec. Cryst. Liq. Cryst*, **413** , 305-320, 2004

[5] G. Dangelmayr and I. Oprea, Eckhaus Stability Boundaries for Waves in Anisotropic Systems, *In Preparation*, 2005

[6] G. Dangelmayr and L. Kramer, Mathematical tools for pattern formation, in *Evolution of Spontaneous Structures in Dissipative Continuous Systems*, (F. Busse and S.C. Müller eds.), Springer, 1-85, 1998

[7] G. Dangelmayr and B. Fiedler and K. Kirchgässner and A. Mielke, *Dynamics of Nonlinear Waves in Dissipative Systems: Reduction, Bifurcation and Stability*, Addison Wesley Longman Ltd., 1996

[8] M. Dennin and D.S. Cannel and G. Ahlers, Patterns in Electroconvection in the Nematic Liquid Crystal I52, *Mollec. Cryst. Liq. Cryst.*, **261**, 337,1995

[9] M. Dennin and G. Ahlers and D.S. Cannell, Chaotic Localized States near the Onset of Electroconvection, *Physical Review Letters,* **77**, 2475, 1996

[10] W. Helfrich, Conduction-induced Alignment of nematic Liquid Crystals: Basic Model and Stability Considerations *J. Chem. Phys.*, **51**, 4092-4105, 1969

[11] L. Kramer and W. Pesch, Convection Instabilities in Nematic Liquid Crystals, in *Macromolecular Systems: Microscopic Interactions and Macroscopic Properties*, (H. Hoffmann and M. Schwoerer and T. Vogtmann eds.), Wiley, 250-294, 2000

[12] M. Silber and H. Riecke and L. Kramer, Symmetry breaking Hopf bifurcation in anisotropic systems, *Physica D*, **61**, 260, 1992

[13] Treiber, M. and L. Kramer, Coupled complex Ginzburg-Landau equations for the weak electrolyte model of electroconvection, *Physical Review E* **58**, 1973, 1998

[14] M. Treiber, On the Theory of the Electrohydrodynamic Instability in Nematic Liquid Crystals near Onset, University of Bayreuth, PhD Dissertation, Department of Physics, 1996

[15] M. Wegelin, Nichtlineare Dynamik raumzeitlicher Muster in hierarchischen Systemen, University of Tübingen, PhD Dissertation, Department of Physics, 1993

[16] B. Werner, Numerical computation of degenerate Hopf bifurcation points, ZAMM, **78**, 807-821, 1998

[17] W. Zimmermann and L. Kramer, Oblique-roll Electrodynamic in Nematics, *Physical Review Letters* **55**, 402, 1985